



 Cite this: *RSC Adv.*, 2021, 11, 16351

Whether planar or corrugated graphitic carbon nitride combined with titanium dioxide exhibits better photocatalytic performance?

 Nguyen Thi Thu Ha, ^a Pham Thi Be,^{ab} Phung Thi Lan,^a Nguyen Thi Mo,^a Le Minh Cam^a and Nguyen Ngoc Ha*^a

The density functional theory method was performed to study the electronic structures of planar (pGN), corrugated (cGN) graphitic carbon nitride and their interactions with titanium dioxide cluster (TiO₂)₇. The transfer of photoinduced electrons was analyzed and electronic excitations were calculated. The obtained results show that cGN is thermodynamically more stable than pGN. cGN chemically interacts with titanium dioxide clusters, while the interaction between pGN and the cluster is assigned to physical nature. The combination of cGN and pGN with (TiO₂)₇ reduces the energy of the first excited states compared to that of the pure substances. The photocatalytic activities were estimated based on hypotheses on the location of the reduction and oxidation sites, the distance between the photoinduced holes and electrons and the electron density of molecular orbitals involved in the excitation. cGN/TiO₂ is predicted to have a higher photocatalytic activity than pGN/TiO₂.

Received 15th February 2021

Accepted 18th April 2021

DOI: 10.1039/d1ra01237a

rsc.li/rsc-advances

Introduction

Graphitic carbon nitride (g-C₃N₄) is a relatively new type of carbon-based material that is being researched in the last few decades. g-C₃N₄ possesses many unique properties such as non-toxicity, high thermal and chemical stability, simplicity of fabrication techniques, moderate band gap, which make it a promising candidate in electronic, catalytic and energetic applications.^{1,2} In particular since Wang and his co-workers first discovered the photocatalytic H₂ and O₂ evolution by water splitting over g-C₃N₄ in 2009,³ g-C₃N₄ has gained tremendous attention as an organic semiconductor metal-free photocatalyst. Recently, g-C₃N₄ has been widely investigated for the photodegradation of organic pollutants,^{4–6} water splitting,^{7,8} CO₂ conversion,^{9–11} *etc.* However, high electron-hole pair recombination rate and insufficient visible absorption are principal drawbacks of g-C₃N₄. Many efforts have been devoted to overcoming these two deficiencies by modifying the electronic band structure of g-C₃N₄ through methods such as metal ion doping,¹² non-metal doping,¹³ noble metal-loading^{9,14} or creating heterojunction structures with other semiconductors.^{10,11,15,16} The latter has been shown to be an effective method for improving photocatalytic performance through better charge separation at the interface between two semiconductors since valence and conduction bands (VB and CB) of one semiconductor are located at higher energy levels compared to those of other coupling semiconductors. The

popular semiconductor widely used for coupling with g-C₃N₄ is a traditional photocatalyst – titanium dioxide (TiO₂). The combination of g-C₃N₄ and TiO₂ (g-C₃N₄/TiO₂) has shown to exhibit higher photocatalytic activity compared to that of pure materials in many reactions due to the efficient separation of the photogenerated electron-hole pairs.^{15,17–22} However, the inside mechanism of electron transfer in the g-C₃N₄/TiO₂ combination and the interaction between components are still rarely discussed in the literature. Wang *et al.* studied TiO₂-C₃N₄ hybrid microspheres²¹ and found that this hybrid material exhibited superior photocatalytic activity compared to TiO₂-C₃N₄ composites prepared by traditional physical mixing methods. In the FTIR spectrum of the hybrid material, some location shifts of C₃N₄ characteristic bands were observed, suggesting the presence of chemical interaction or a synergistic effect between TiO₂ and C₃N₄. Fagan *et al.* studied photocatalytic properties of g-C₃N₄/TiO₂ heterojunctions²² and reported a substantial up-field shift in Raman spectra upon the addition of g-C₃N₄ to TiO₂, indicating the formation of new bonds or bond modifications. Therefore, the authors suggested that g-C₃N₄ was probably incorporated into the TiO₂ system rather than existing as a component of the mixture of the two.¹⁹

The structural and optical properties of the g-C₃N₄/TiO₂ system have also been intensively investigated in various theoretical studies.^{15,19,20,23,24} Lin *et al.* studied the electronic and optical properties of g-C₃N₄/TiO₂(101) heterostructure using

^aFaculty of Chemistry, Hanoi National University of Education, 136 Xuan Thuy Str., Hanoi, Vietnam. E-mail: hann@hnue.edu.vn

^bFaculty of Natural Science and Technology, Taynguyen University, Daklak, Vietnam


spin-polarized DFT+U calculations.¹⁵ Based on the calculated equilibrium distance between g-C₃N₄ and anatase TiO₂(101) (1.94 Å) and the binding energy (24 meV Å⁻²), the g-C₃N₄/TiO₂(101) composite material was assigned to the van der Waals heterostructure. The authors also noticed that the electrons can migrate from the g-C₃N₄ monolayer to anatase TiO₂ (101) surface, which leads to oxidation and redox reactions occurring on g-C₃N₄ and TiO₂, respectively. A similar charge transfer was reported in the work of Liu *et al.*²⁰ The interaction between TiO₂ and g-C₃N₄ results in the formation of a built-in electric field at the interface, which encourages the separation of electron-hole pairs.^{15,19,20} Gao *et al.* suggested that electron transition from the highest occupied molecular orbital (HOMO) to the lowest unoccupied molecular orbital (LUMO) promoted the separation of electrons and holes.¹⁹

Obviously, the interaction between TiO₂ and g-C₃N₄ plays a crucial role in the photocatalytic performance of the combined material. It is also has been reported in various studies that the structure of the material, including deficient structures of g-C₃N₄, significantly influences its catalytic activity.^{25–28} Lei *et al.* studied a TiO₂/g-C₃N₄ composite photocatalyst with an inverse opal structure and heterojunction²⁸ and showed that the inverse opal TiO₂/g-C₃N₄ degraded Rhodamine B 2.7 times faster than the normal TiO₂/g-C₃N₄, owing to the interaction between inverse opal g-C₃N₄ and TiO₂ creating more interfaces for the efficient transfer of photogenerated electron-hole pairs.²⁹ Ren *et al.* studied stabilities, electronic properties, and nitrogen reduction activity of planar and corrugated conformations of g-C₃N₄ (ref. 25) and showed the distortion conformation could activate more $n \rightarrow \pi^*$ transitions of g-C₃N₄, promoting

separation efficiency of photoinduced carriers in g-C₃N₄. The stability of the corrugated geometry of g-C₃N₄ compared to the planar geometry was highlighted in several theoretical studies. The corrugation was proved to minimize the electronic repulsion experienced by the N lone pairs located in their structural holes.^{29,30} It was suggested that the corrugation enhances the catalytic performance of g-C₃N₄ for the selective production of CO/CH₃OH.³⁰

In this work, we investigate the interaction between the planar and corrugated g-C₃N₄ with titanium dioxide cluster and clarify the mechanism of the transfer of photogenerated electrons using a combination of different theoretical methods.

Models and computational methods

Models. It is well known that the two main forms of g-C₃N₄ are triazine and heptazine (tri-s-triazines), which can simultaneously exist.³¹ This work focuses on triazine-based g-C₃N₄, which is used to build corrugated (denoted as cGN) and in planar (denoted as pGN) forms. The idea of studying the corrugated and planar forms of g-C₃N₄ is because the synthesized g-C₃N₄ has a multilayer structure. The surface of g-C₃N₄ can be considered corrugated if the material has a thin structure. In contrast, if the thickness of g-C₃N₄ is thick enough, the surface can be considered planar.

In both, constructed corrugated and planar models, the peripheral atoms were saturated by hydrogen atoms. cGN and pGN consist of 200 atoms and have a molecular formula of C₇₅N₁₀₀H₂₀.

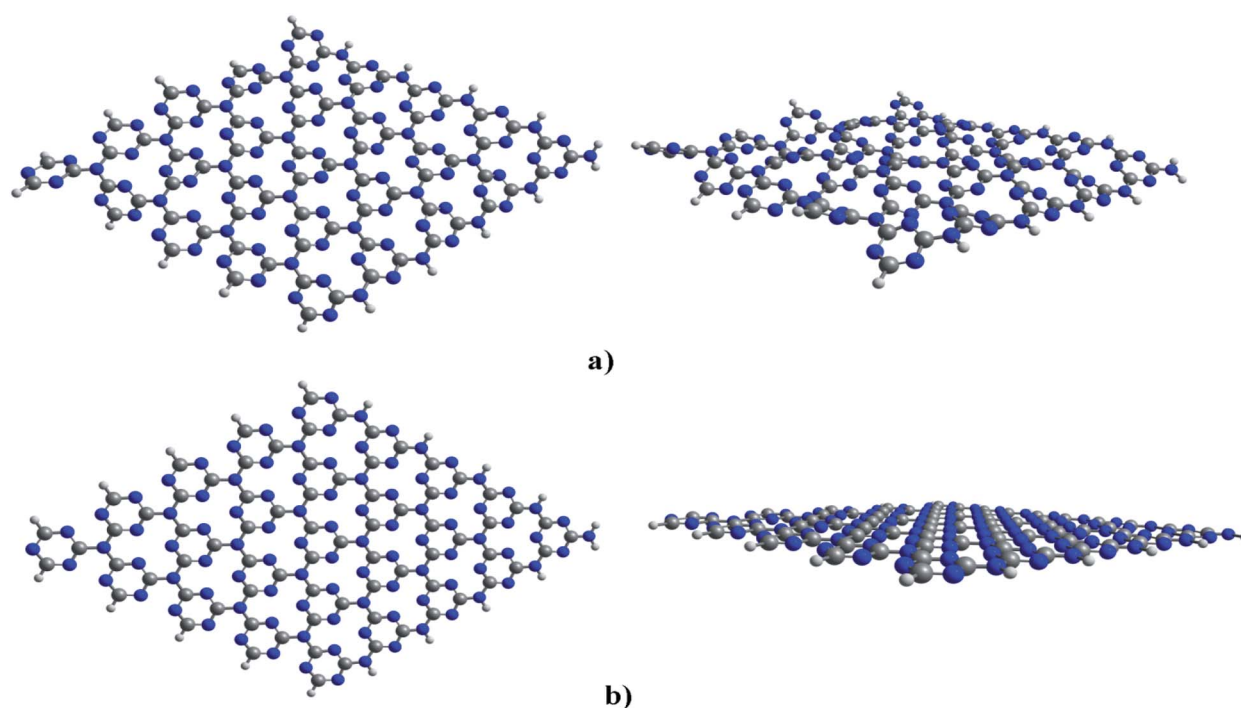


Fig. 1 Optimized structures of cGN (a) and pGN (b); colours: grey-carbon, blue-nitrogen; key distances are in Å.



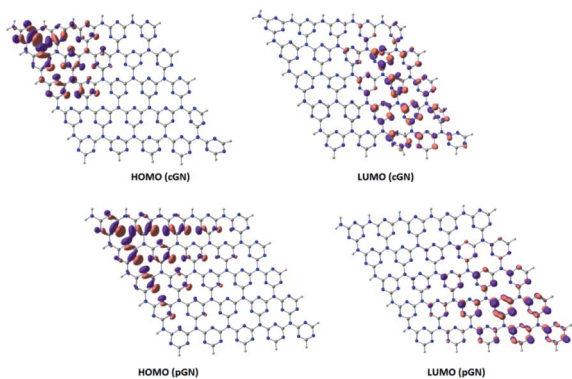


Fig. 2 HOMO and LUMO of cGN (a) and pGN (b) depicted at an isovalue of $0.03 \text{ e } \text{Å}^{-3}$.

Titanium dioxide cluster (TiO_2)₇ was chosen due to the comparable stability among small (TiO_2)_n clusters ($n = 1-9$) in terms of cluster formation energy per TiO_2 unit.³² The initial geometry of the (TiO_2)₇ cluster was created from the anatase structure of the bulk.

Computational methods. All optimization and energy calculations were performed using the DFT approach in the generalized gradient approximation (GGA). The PBE (Perdew, Burke, and Ernzerhof) gradient-corrected function was used to calculate the exchange–correlation energy.³³ The double zeta basis plus polarization orbitals (DZP) was used for valence electrons, while core electrons were treated by using norm-conserving pseudopotentials in its fully nonlocal (Kleinman–Bylander) form.³⁴ The spin-polarized function, which performs a calculation with collinear spin was applied in all calculations, and, thus, the total spin polarization for an optimized structure was automatically determined for the structure with the lowest energy. The calculations have been performed using the SIESTA code.³⁵

UV-Vis spectra were calculated using time-dependent-density functional theory (TD-DFT) at CAM-B3LYP/6-31G(d,p) level of theory. This method is implemented in the ORCA

code.^{36,37} The energy threshold up to which configuration state functions (CSFs) included is 8 eV.

Results and discussions

Electronic structures of cGN, pGN and (TiO_2)₇

cGN and pGN. The optimized structures of cGN and pGN are presented in Fig. 1.

The calculated results show that cGN has an energy of 9.2 eV, lower than that of pGN. In other words, cGN is more stable than pGN in terms of the formation energy. The corrugation in the structure of cGN is attributed to the strong repulsion between nitrogen atoms, which are in the sp^2 hybridization state and contain valence electron pairs in the xOy plane.³⁰ This finding is consistent with previous studies.^{29,30}

Analysis of HOMO and LUMO provides useful information about the photogenerated electrons. Fig. 2 illustrates HOMO and LUMO of cGN and pGN. Notably, the multiplicity of both cGN and pGN is 1, implying that the systems do not have unpaired electrons.

The distribution of HOMO and LUMO of cGN and pGN is very similar. In cGN, as well as in pGN, HOMO is mainly located on the nitrogen atoms in the triazine heterocycles (denoted as N1 atoms), while the three-coordinated (linked) nitrogen atoms (denoted as N2 atoms) almost do not contribute to HOMO. The LUMO is primarily supported by N1 and carbon atoms in the heterocycles. It is noted that LUMO is perpendicular to the molecular plane.

When a molecule absorbs light with appropriate energy, electrons can be excited from the occupied molecular orbitals (H) to the unoccupied molecular orbitals (L) to form photo-generated holes (h^+) and electrons (e^*), as illustrated in the following scheme:



Table 1 The parameters of the first excitation of g-C₃N₄

	Excitation energy, eV	Oscillator strength $f \times 10^4$	The amplitude of MO transition		
cGN	4.185	9.93	0.07 (HOMO-4 → LUMO)	0.06 (HOMO-4 → LUMO+3)	0.06 (HOMO-1 → LUMO+1)
pGN	3.769	7.07	0.11 (HOMO-1 → LUMO+12)	0.08 (HOMO → LUMO+22)	0.06 (HOMO → LUMO+15)

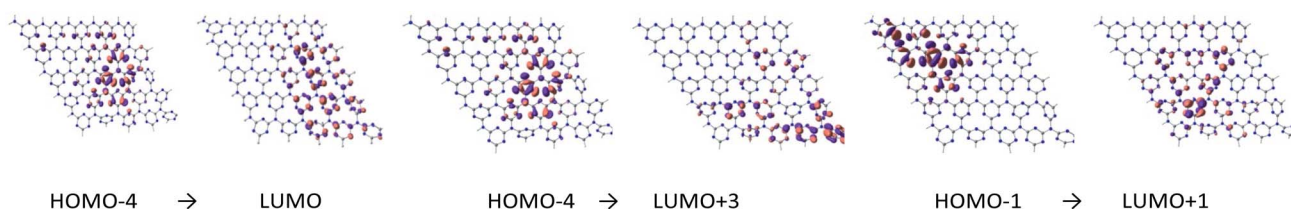


Fig. 3 Molecular orbitals involved in the first excitation of cGN depicted at an isovalue of $0.03 \text{ e } \text{Å}^{-3}$.



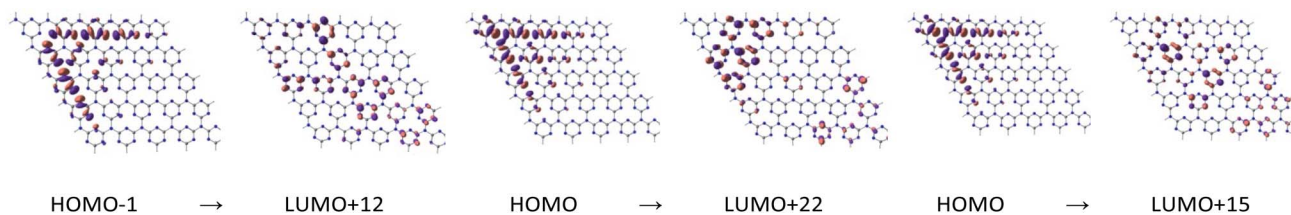


Fig. 4 Molecular orbitals involved in the first excitation of pGN depicted at an isovalue of $0.03 \text{ e } \text{\AA}^{-3}$.

The h^+e^* pair will play the critical role of an oxidant and a reductant in photocatalysis reactions.

An effective photocatalyst is a material that satisfies the following two requirements: (i) the recombination rate of h^+ and e^* is low and (ii) h^+ and e^* can be generated under visible light irradiation.

Starting from the first requirement, we propose three hypotheses for the explanation of an effective separation of h^+ and e^* :

(i-a): The reduction and oxidation sites are located separately to facilitate photocatalytic reactions,

(i-b): The greater the distance between h^+ and e^* is, the more efficient the separation is,

(i-c): The electron density of H (where h^+ is formed) as well as L (where e^* is generated) in narrow space results in high densities of h^+ and e^* , which would be more effective for the electron transfer process.

The HOMO and LUMO of the cGN system (Fig. 2) are located in different spatial areas and spread across many atoms. As a result, the photogenerated electrons and holes are far apart from each other, leading to their efficient separation and slow recombination. A similar picture is observed for the pGN system. These specific structural features along with the moderate band gap properly contribute to the photocatalytic activity of $g\text{-C}_3\text{N}_4$.

To study the nature of the excitation of $g\text{-C}_3\text{N}_4$, TD-DFT calculations were performed. The results are summarized in Table 1. Fig. 3 and 4 illustrate molecular orbitals involved in the first excitation of cGN and pGN. The excitation energy of the first excited state was used instead of the bandgap to evaluate the photocatalytic activity. In principle, a photocatalytic process is initiated with the photon absorption of the photocatalyst to generate the first excited state. The calculation results show that cGN has 2070 roots (excitations) and pGN has 2190 roots. The excitation energies of the first excited states of gCN and pCN were determined to be 4.185 eV and 3.769 eV, respectively. It is also noted that the theoretical band gap is strongly dependent on the model size due to the quantum confinement effect.^{38,39} Hence, using the energy of the first excited state is meaningful for the same size of the $g\text{-C}_3\text{N}_4$ model used.

H and L involved in the first excitation of cGN are distributed in a narrower space than those of pGN. Although the excitation energy of the first excited state of cGN is slightly larger than that of pGN, according to the above-proposed hypothesis (i-c), cGN form is predicted to have higher photocatalytic activities than

the pGN form. This finding is consistent with the previous studies.^{25,30}

To estimate the photoexcitation probability, fractional occupation density (FOD) was calculated and analyzed. The FOD analysis provides meaningful information about the static correlated electrons, *viz.* active electrons in a molecule.^{40,41} The fractional occupation number weighted electron density (ρ^{FOD}) at r position is defined as:

$$\rho^{\text{FOD}}(r) = \sum_i^N (\delta_1 - \delta_2 f_i) |\varphi_i(r)|^2 \quad (2)$$

where φ_i are molecular spin orbitals, f_i is the fractional orbital occupation number ($0 \leq f_i \leq 1$) and the sum is taken over all electronic single-particle levels in the system. The fractional occupation number f_i is calculated as:

$$f_i = \frac{1}{e^{(\epsilon_i - E_F)/kT_{el}} + 1} \quad (3)$$

where E_F is the Fermi energy level, T_{el} is the electron temperature. The constants δ_1 and δ_2 are chosen to be unity if the level is lower than E_F , while they are zero and -1 , respectively, for levels higher than E_F .^{40,41}

The larger the FOD of an atom is, the more active is the atom considered. From the results of FOD calculations for cGN at $T_{el} = 12500 \text{ K}$, it can be seen that the nitrogen and carbon atoms in the triazine heterocycles are more active with FOD equal to 0.32 and 0.20 e per bohr³, respectively. Meanwhile, the linked three coordinated nitrogen atoms outside the ring have a FOD value of only about 0.10 e per bohr³. These results are consistent with the above-discussed contribution of atoms of $g\text{-C}_3\text{N}_4$ into HOMOs and LUMOs. Thus, photoinduced electrons are likely to come from N and C atoms in the heterocycles.

Titanium dioxide (TiO_2)₇. Fig. 5 illustrates the HOMO and LUMO of the $(\text{TiO}_2)_7$ cluster. Obviously, the HOMO of $(\text{TiO}_2)_7$

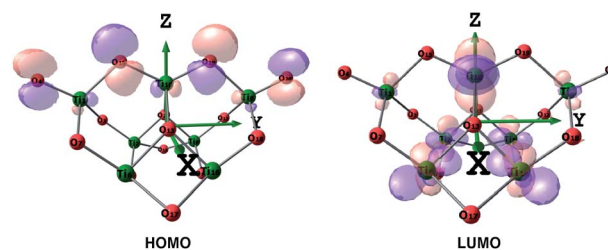
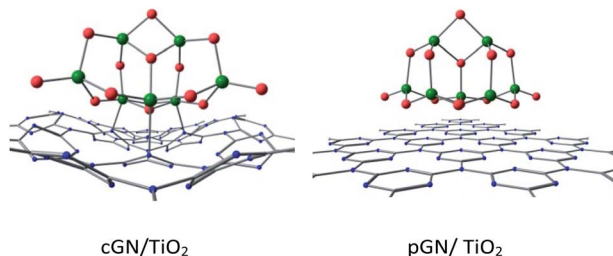


Fig. 5 HOMO and LUMO of the $(\text{TiO}_2)_7$ cluster depicted at an isovalue of $0.05 \text{ e } \text{\AA}^{-3}$, colours: red-oxygen, green-titanium.



Table 2 The parameters of the first excitation of (TiO₂)₇

	Excitation energy (eV)	Oscillator strength $f \times 10^4$	The amplitude of MO transition		
(TiO ₂) ₇	4.738	7.67	0.88 (HOMO → LUMO)	0.03 (HOMO → LUMO+12)	0.03 (HOMO → LUMO+3)

Fig. 6 Optimized structures of the most favorable configurations of cGN/TiO₂ and pGN/TiO₂.

cluster is mainly supported by 2p_z orbitals of oxygen atoms with the sum of the squares of the coefficients in the wavefunction's equation was determined to be 0.84. In contrast, the LUMO of (TiO₂)₇ cluster was primarily contributed by 3d orbitals of titanium atoms with the sum of the squares of the coefficients in the LUMO's equation equal to 0.70 (considering only 3d orbitals with coefficients larger than 0.10).

Thus, when TiO₂ absorbs photons, electrons will transfer from O atoms contributing to HOMO to Ti atoms, contributing to LUMO. It is noted that in the Frontier HOMO and LUMO of the TiO₂ cluster, contributions of O atoms at different positions to HOMO (and similarly for Ti atoms to LUMO) are different, which is attributed to the different mobility of the atoms.

The excitation energy of the first excited state of (TiO₂)₇ is 4.738 eV. The calculation results for the first excited state of (TiO₂)₇ are tabulated in Table 2.

Thus, for the (TiO₂)₇ cluster, the transition from HOMO to LUMO primarily contributes to the first excitation. Unlike g-C₃N₄, TiO₂ is typically considered chemically inert, *i.e.*, it does not react with other substances and is, therefore, a stable substance that can be used in many different industries and in a variety of applications. This is an important property contributing to the broad practical application of TiO₂. However, the drawback of using anatase in photocatalytic applications lies in its large bandgap. Therefore, the combination of TiO₂ with g-C₃N₄ is expected to decrease the band gap compared to that in pure substances.

Combination of g-C₃N₄ and TiO₂

Interaction between cGN and pGN with (TiO₂)₇. When (TiO₂)₇ is placed onto the g-C₃N₄ structure, there are a number of possible configurations. In this work, the most favorable configurations for g-C₃N₄/TiO₂ systems were preliminarily determined using the iMTD-GC algorithm, which makes use of extensive metadynamic sampling (MTD), with an additional genetic z-matrix crossing (GC) step at the end. iMTD-GC is

implemented in the GFN-xTB (short for "Geometries, Frequencies, and Noncovalent interactions-extended TightBinding") package.^{42–44} The generated favorable configurations from iMTD-GC calculations were then fully optimized at GGA-PBE/DZP level of theory. Fig. 6 illustrates the most favorable configurations of cGN and pGN combined with the (TiO₂)₇ cluster, which are denoted as cGN/TiO₂ and pGN/TiO₂, respectively.

The interaction between cGN and pGN with (TiO₂)₇ cluster is characterized by the interaction energy ($\Delta_{\text{int}}E$), which is defined as follows:

$$\Delta_{\text{int}}E = E(\text{gC}_3\text{N}_4/\text{TiO}_2) - E(\text{gC}_3\text{N}_4) - E(\text{TiO}_2)$$

The interaction energy determined for cGN/TiO₂ and pGN/TiO₂ was $-355.9 \text{ kJ mol}^{-1}$ and $-185.0 \text{ kJ mol}^{-1}$, respectively. Thus, the formation of g-C₃N₄/TiO₂ systems is energetically favorable. To evaluate the nature of the interaction between g-C₃N₄ and TiO₂ cluster, Mayer bond order (BO) was calculated and analyzed using the following definition:

$$\text{BO}(\text{AB}) = \sum_{\mu \in \text{A}} \sum_{\nu \in \text{B}} [(PS)_{\mu\nu} + (PS)_{\nu\mu} + (RS)_{\mu\nu} + (RS)_{\nu\mu}]$$

where, P is the total electron density matrix, R is the spin-density matrix and S is the overlap matrix.

The computed BO, distances between atoms (d) and Hirshfeld net atomic charge (q) for cGN/TiO₂ and pGN/TiO₂ are presented in Table 3.

It can be seen that, for the cGN/TiO₂ combination, the distances between Ti and N atoms are slightly larger than the sum of the atomic radius of Ti and N (2.05 Å). This finding is consistent with the reasonable values of BO between Ti atoms and N atoms, which are smaller than 1. A significant charge transfer from cGN to (TiO₂)₇ is observed. Thus, the interaction between cGN and TiO₂ clusters is considered to have a chemical nature.

Table 3 Calculation results for cGN/TiO₂ and pGN/TiO₂

Parameters	cGN/TiO ₂	pGN/TiO ₂
BO	BO(Ti1–N) = 0.386 BO(Ti2–N) = 0.384 BO(Ti3–N) = 0.362	BO(Ti–N) = 0.015–0.071 BO*(Ti–N) = 0.183
d , Å	$d(\text{Ti1–N}) = 2.235$ $d(\text{Ti1–N}) = 2.243$ $d(\text{Ti1–N}) = 2.327$	$d(\text{Ti–N}) = 3.200$
$q(\text{TiO}_2)_7$, e	–1.019	–0.741



Table 4 Parameters of the first excitation of cGN/TiO₂ and pGN/TiO₂

	Excitation energy (eV)	Oscillator strength $f \times 10^4$	The amplitude of MO transition		
cGN/TiO ₂	3.712	7.67	0.34 (HOMO → LUMO+1)	0.10 (HOMO-7 → LUMO+1)	0.08 (HOMO-6 → LUMO+1)
pGN/TiO ₂	2.206	2.25	0.16 (HOMO-5 → LUMO)	0.15 (HOMO-3 → LUMO)	0.11 (HOMO-2 → LUMO)

For the pGN/TiO₂ combination, the minimum distance between Ti atoms of the TiO₂ cluster and N atoms of g-C₃N₄ was determined to be 3.2 Å, which is significantly larger than the sum of the atomic radii of Ti and N. The BO between Ti and N atoms is quite small and ranges from 0.015 to 0.071 and the total BO between Ti and N atoms is only 0.183. The charge transfer from pGN to (TiO₂)₇ is less than from cGN to (TiO₂)₇. Therefore, it can be suggested that the interaction between the TiO₂ cluster and pGN is primarily governed by physical interactions. These findings are in good agreement with the work of Lin *et al.*, who reported that the interaction between g-C₃N₄ and anatase TiO₂ (101) is assigned to the van der Waals heterostructure.¹⁵ This can make the photocatalytic performance of pGN/TiO₂ very different compared to that of the cGN/TiO₂ combination.

Electronic excitation. The excitation energies of the first excited states are 3.712 eV and 2.206 eV for cGN/TiO₂ and pGN/TiO₂, respectively. Table 4 and Fig. 7 illustrate the contribution of molecular orbitals transition to the first excitation of cGN/TiO₂ and pGN/TiO₂.

The calculation results show that the first excitation of cGN/TiO₂ is primarily determined by the transfer of photogenerated electrons from the HOMOs (HOMO, HOMO-7, HOMO-6),

mainly located on g-C₃N₄ to the LUMO+1 orbital principally contributed from d orbitals of Ti and 2p_z orbitals of N atoms. Electrons from cGN/TiO₂ could be photogenerated by photons with an energy of 3.712 eV, which is much lower than the case of pure cGN and the TiO₂ clusters. Moreover, HOMOs and LUMO+1 orbitals of cGN/TiO₂ are distributed in different spatial areas. When photogenerated electrons are assigned to TiO₂, their density is higher as compared to the distribution of these electrons on the large cGN surface and, thus, makes the electron transfer process more favorable.

The calculated HOMO and LUMO energy levels are -10.575 and -2.406 eV, and, -7.964 and -1.054 eV for the TiO₂ cluster and cGN, respectively. There is an important issue that will be clarified: how do electrons transfer from g-C₃N₄ to TiO₂ when photogenerated? If the interaction between g-C₃N₄ and TiO₂ is just physical, electrons cannot migrate because both g-C₃N₄ and TiO₂ are non-metal. If there is a strong chemical interaction, the electronic structure of each substance will be changed, leading to photocatalytic deactivity.

For the cGN/TiO₂ system, the interaction between TiO₂ and cGN is considered as a weak chemical interaction expressed through a small BO and the atomic distances and, thus, the LUMO+1 orbital of the cGN/TiO₂ system contains both 2p_z

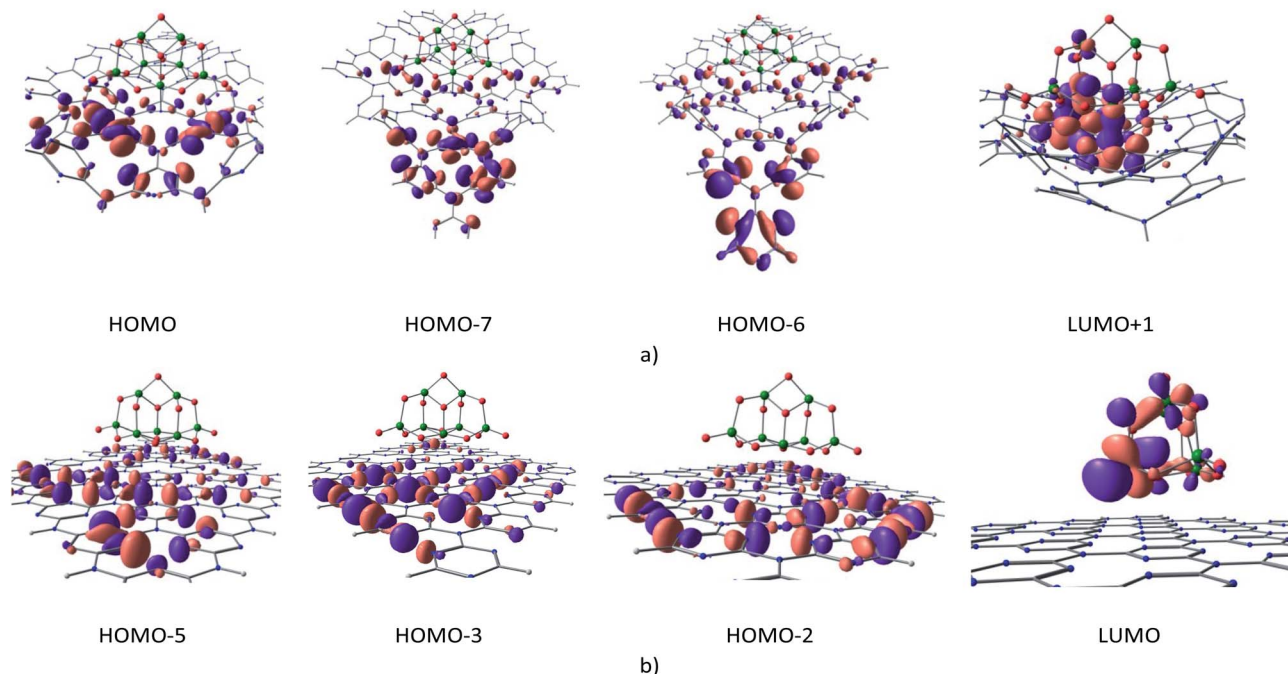


Fig. 7 Molecular orbitals involved in the first excitation of cGN/TiO₂ (a) and pGN/TiO₂ (b) depicted at an isovalue of 0.03 e Å⁻³.



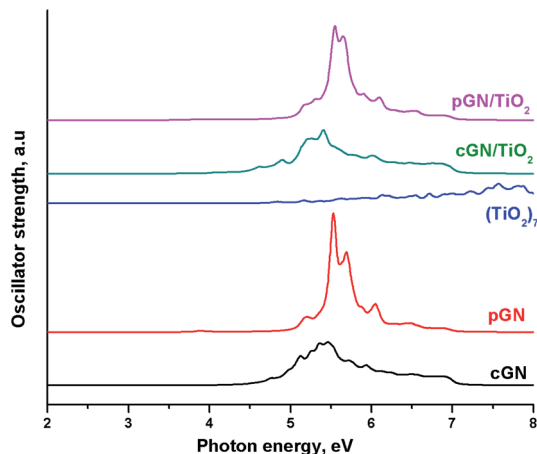


Fig. 8 Calculated UV-Vis spectra of cGN/TiO₂ and pGN/TiO₂.

orbitals of N atoms and 3d orbitals of Ti atoms. Therefore, the electron transition in cGN/TiO₂ can be described as follows: cGN, due to the lower energy of the first excited state as compared to TiO₂, when photogenerated, electrons transfer from the hybrid orbitals containing electron pairs of the N atoms in HOMOs (H) to the 2p_z orbitals of N atoms in (LUMO+1) orbitals. This transition is the same as described for g-C₃N₄ (Fig. 2), but the difference is that electrons transfer only to 2p_z orbitals of N atoms bound to Ti atoms. Both the 2p_z orbitals of N atoms and the 3d orbitals of Ti atoms are involved in the (LUMO+1) orbital, so in this case, the electron transition is almost instantaneous.

For the pGN/TiO₂ system, the LUMO system consists of only orbitals of the TiO₂ cluster. Because there is no chemical interaction between pGN and the TiO₂ cluster, there is no electron transfer from pGN to TiO₂. Thus, for the pGN/TiO₂ system, although the energy of the first excited state is reduced, the photocatalytic efficiency of the combined system is not significantly improved compared to the pure substances.

The calculated UV-Vis spectra for (TiO₂)₇, cGN, pGN compared with UV-Vis of cGN/TiO₂ and pGN/TiO₂ are illustrated in Fig. 8. The relative total peak areas (*S*) in the photon energy region of 2–5 eV for the studied systems are shown in Table 5.

The UV-Vis of pGN/TiO₂ is not different from the parent pGN, proving that there is no chemical interaction between (TiO₂)₇ and pGN. Meanwhile, the spectrum of cGN/TiO₂ has a significant shift to the lower energy photon region. This is attributed to the above-mentioned interaction between (TiO₂)₇ and cGN. Besides, cGN/TiO₂ exhibits a larger total peak area than that of the pure components and thus, more transitions are appearing in the photon energy region of 2–5 eV. The combination between TiO₂ and cGN improved the light

absorption ability of the component due to the synergistic effect. Concerning the idea of using corrugated and planar models of g-C₃N₄ that characterize the thickness of the material (see section Models), our calculation results confirm that exfoliated g-C₃N₄ nanosheets exhibit higher photocatalytic performance than bulk C₃N₄. These findings are in good agreement with the experimental study of Gao *et al.* on the enhancement of the photocatalytic activity of ZnO/g-C₃N₄ composites by regulating the stacked thickness of g-C₃N₄ nanosheets.⁴⁵ Their results showed that ZnO/g-C₃N₄ with the middle thickness shows the highest photocatalytic performance.

Conclusions

The interactions between planar g-C₃N₄ (pGN) and corrugated g-C₃N₄ (cGN) with the (TiO₂)₇ cluster were investigated using the DFT method. The obtained findings show that the cGN chemically interacts with the titanium cluster, while the interaction between pGN and the cluster is assigned to physical nature. The combination of both cGN and pGN with (TiO₂)₇ reduces the energy of the first excited state. The photocatalytic activities were estimated based on hypotheses on the location of the photoinduced holes and electrons and the electron density of the molecular orbitals involved during excitation. cGN/TiO₂ is predicted to have a higher photocatalytic activity than pGN/TiO₂ due to the synergistic effect.

Author contributions

Conceptualization: Nguyen Ngoc Ha; data curation: Nguyen Thi Thu Ha, Pham Thi Be, formal analysis: Nguyen Thi Thu Ha, Phung Thi Lan, Nguyen Thi Mo and Pham Thi Be, investigation: Nguyen Thi Thu Ha, Nguyen Ngoc Ha, Phung Thi Lan, Nguyen Thi Mo and Pham Thi Be; methodology: Nguyen Ngoc Ha, Le Minh Cam and Nguyen Thi Thu Ha; project administration: Nguyen Ngoc Ha; visualization: Phung Thi Lan, Nguyen Thi Mo and Pham Thi Be; writing – original draft: Nguyen Thi Thu Ha, Pham Thi Be, Phung Thi Lan and Nguyen Thi Mo; writing – review & editing: Nguyen Ngoc Ha and Le Minh Cam.

Conflicts of interest

There are no conflicts to declare.

Acknowledgements

This research is funded by Vietnam National Foundation for Science and Technology Development (NAFOSTED) under grant number 05/2018/TN.

Notes and references

- 1 A. Wang, C. Wang, L. Fu, W. Wong-Ng and Y. Lan, *Nano-Micro Lett.*, 2017, **9**, 1–21.
- 2 G. Dong, Y. Zhang, Q. Pan and J. Qiu, *J. Photochem. Photobiol., C*, 2014, **20**, 33–50.

Table 5 Relative total peak area (*S*) in the photon energy region of 2–5 eV for (TiO₂)₇, cGN, pGN, cGN/TiO₂ and pGN/TiO₂

System	(TiO ₂) ₇	cGN	pGN	cGN/TiO ₂	pGN/TiO ₂
<i>S</i>	1.0	91.4	32.2	117	38.8



- 3 X. Wang, K. Maeda, A. Thomas, K. Takanebe, G. Xin, J. M. Carlsson, K. Domen and M. Antonietti, *Nat. Mater.*, 2009, **8**, 76–80.
- 4 Z. Chen, S. Zhang, Y. Liu, N. S. Alharbi, S. O. Rabah, S. Wang and X. Wang, *Sci. Total Environ.*, 2020, **731**, 139054.
- 5 Y. Wei, Q. Zou, P. Ye, M. Wang, X. Li and A. Xu, *Chemosphere*, 2018, **208**, 358–365.
- 6 P. Wang, S. Sun, X. Zhang, X. Ge and W. Lü, *RSC Adv.*, 2016, **6**, 33589–33598.
- 7 H. Ma, J. Feng, F. Jin, M. Wei, C. Liu and Y. Ma, *Nanoscale*, 2018, **10**, 15624–15631.
- 8 S. Ye, R. Wang, M. Z. Wu and Y. P. Yuan, in *Applied Surface Science*, Elsevier B.V., 2015, vol. 358, pp. 15–27.
- 9 W. J. Ong, L. L. Tan, S. P. Chai and S. T. Yong, *Dalton Trans.*, 2014, **44**, 1249–1257.
- 10 Y. He, Y. Wang, L. Zhang, B. Teng and M. Fan, *Appl. Catal., B*, 2015, **168–169**, 1–8.
- 11 J. Wang, C. Qin, H. Wang, M. Chu, A. Zada, X. Zhang, J. Li, F. Raziq, Y. Qu and L. Jing, *Appl. Catal., B*, 2018, **221**, 459–466.
- 12 S. Wojtyła, K. Śpiewak and T. Baran, *J. Inorg. Organomet. Polym. Mater.*, 2020, **30**, 3418–3428.
- 13 W. Xing, G. Chen, C. Li, Z. Han, Y. Hu and Q. Meng, *Nanoscale*, 2018, **10**, 5239–5245.
- 14 X. B. Qian, W. Peng and J. H. Huang, *Mater. Res. Bull.*, 2018, **102**, 362–368.
- 15 Y. Lin, H. Shi, Z. Jiang, G. Wang, X. Zhang, H. Zhu, R. Zhang and C. Zhu, *Int. J. Hydrogen Energy*, 2017, **42**, 9903–9913.
- 16 S. Adhikari and D. H. Kim, *Appl. Surf. Sci.*, 2020, **511**, 145595.
- 17 M. A. Alcudia-Ramos, M. O. Fuentez-Torres, F. Ortiz-Chi, C. G. Espinosa-González, N. Hernández-Como, D. S. García-Zaleta, M. K. Kesarla, J. G. Torres-Torres, V. Collins-Martínez and S. Godavarthi, *Ceram. Int.*, 2020, **46**, 38–45.
- 18 R. Acharya and K. Parida, *J. Environ. Chem. Eng.*, 2020, **8**, 103896.
- 19 H. Gao, J. Jia, F. Guo, B. Li, D. Dai, X. Deng, X. Liu, C. Si and G. Liu, *J. Photochem. Photobiol., A*, 2018, **364**, 328–335.
- 20 J. Liu, B. Cheng and J. Yu, *Phys. Chem. Chem. Phys.*, 2016, **18**, 31175–31183.
- 21 W. Wang, Y. Liu, J. Qu, Y. Chen, M. O. Tadé and Z. Shao, *ChemPhotoChem*, 2017, **1**, 35–45.
- 22 R. Fagan, D. E. McCormack, S. J. Hinder and S. C. Pillai, *Materials*, 2016, **9**, 286.
- 23 B. Zhu, B. Cheng, L. Zhang and J. Yu, *Carbon Energy*, 2019, **1**, 32–56.
- 24 H. Gao, B. Lu, D. Li, F. Guo, D. Dai, C. Si, G. Liu and X. Zhao, *RSC Adv.*, 2016, **6**, 65315–65321.
- 25 C. Ren, Y. Zhang, Y. Li, Y. Zhang, S. Huang, W. Lin and K. Ding, *J. Phys. Chem. C*, 2019, **123**, 17296–17305.
- 26 H. Gao, R. Cao, S. Zhang, H. Yang and X. Xu, *ACS Appl. Mater. Interfaces*, 2019, **11**, 2050–2059.
- 27 A. Dandia, S. L. Gupta, P. Saini, R. Sharma, S. Meena and V. Parewa, *Curr. Opin. Green Sustain. Chem.*, 2020, **3**, 100039.
- 28 J. Lei, B. Chen, W. Lv, L. Zhou, L. Wang, Y. Liu and J. Zhang, *Dalton Trans.*, 2019, **48**, 3486–3495.
- 29 D. T. Vodak, K. Kim, L. Iordanidis, P. G. Rasmussen, A. J. Matzger and O. M. Yaghi, *Chem.–Eur. J.*, 2003, **9**, 4197–4201.
- 30 L. M. Azofra, D. R. MacFarlane and C. Sun, *Phys. Chem. Chem. Phys.*, 2016, **18**, 18507–18514.
- 31 L. Zhang, Z. Jin, H. Lu, T. Lin, S. Ruan, X. S. Zhao and Y. J. Zeng, *ACS Omega*, 2018, **3**, 15009–15017.
- 32 A. Zheng-wang Qu and G.-J. Kroes, *J. Phys. Chem. B*, 2006, **110**(18), 8998–9007.
- 33 J. P. Perdew, K. Burke and M. Ernzerhof, *Phys. Rev. Lett.*, 1996, **77**, 3865–3868.
- 34 L. Kleinman and D. M. Bylander, *Phys. Rev. Lett.*, 1982, **48**, 1425–1428.
- 35 J. M. Soler, E. Artacho, J. D. Gale, A. García, J. Junquera, P. Ordejón and D. Sánchez-Portal, *J. Phys.: Condens. Matter*, 2002, **14**, 2745–2779.
- 36 F. Neese, *Wiley Interdiscip. Rev.: Comput. Mol. Sci.*, 2012, **2**, 73–78.
- 37 ORCA Forum – Portal, <https://orcaforum.kofo.mpg.de/app.php/portal>, accessed 13 February 2021.
- 38 S. Furukawa and T. Miyasato, *Phys. Rev. B: Condens. Matter Mater. Phys.*, 1988, **38**, 5726–5729.
- 39 J. Liu, Y. Nie, W. Xue, L. Wu, H. Jin, G. Jin, Z. Zhai and C. Fu, *J. Mater. Res. Technol.*, 2020, **9**, 8020–8028.
- 40 S. Grimme and A. Hansen, *Angew. Chem., Int. Ed.*, 2015, **54**, 12308–12313.
- 41 C. A. Bauer, A. Hansen and S. Grimme, *Chem.–Eur. J.*, 2017, **23**, 6150–6164.
- 42 P. Pracht, F. Bohle and S. Grimme, *Phys. Chem. Chem. Phys.*, 2020, **22**, 7169–7192.
- 43 S. Grimme, C. Bannwarth and P. Shushkov, *J. Chem. Theory Comput.*, 2017, **13**, 1989–2009.
- 44 C. Bannwarth, S. Ehlert and S. Grimme, *J. Chem. Theory Comput.*, 2019, **15**, 1652–1671.
- 45 X. Gao, B. Yang, W. Yao, Y. Wang, R. Zong, J. Wang, X. Li, W. Jin and D. Tao, *Environ. Pollut.*, 2020, **257**, 113577.

